Thin-Walled Structures 166 (2021) 108038

Contents lists available at ScienceDirect

Thin-Walled Structures

journal homepage: www.elsevier.com/locate/tws

Full length article

Debonding development in cracked steel plates strengthened by CFRP laminates under fatigue loading: Experimental and boundary element method analysis

Lili Hu [a,b], Yuanyuan Wang [c], Peng Feng [b,*], HaiTao Wang [d], Hanlin Qiang [b,e]

[a] State Key Laboratory of Ocean Engineering, School of Naval Architecture, Ocean and Civil Engineering, Shanghai Jiao Tong University, Shanghai, 200240, China
[b] Key Laboratory of Civil Engineering Safety and Durability of China Education Ministry, Department of Civil Engineering, Tsinghua University, Beijing 100084, China
[c] China Xiongan Group Co., LTD, Baoding 071700, Hebei Province, China
[d] College of Civil and Transportation Engineering, Hohai University, Nanjing, China
[e] Beijing Municipal Commission of Housing and Urban-rural Development, Beijing 101100, China

ARTICLE INFO

Keywords:
Fatigue
Steel
Carbon fiber reinforced polymer
Debonding
Boundary element method

ABSTRACT

Carbon fiber reinforced polymer (CFRP) laminates can effectively enhance the fatigue life of steel structures. However, few studies have investigated the influence of crack-induced debonding in the CFRP-steel interface on the CFRP strengthening efficiency and the relationship of crack propagation and debonding development. This study experimentally and numerically – with the boundary element method (BEM) – investigated crack propagation and debonding development in CFRP-strengthened cracked steel (Q345, Q460, and Q690) plates. The fatigue test specimens were subjected to a maximum stress of 50% steel yield stress and a stress ratio of 0.1, during which real-time changes in CFRP strain distribution were recorded by digital image correlation (DIC). The CFRP strain gradient calculations showed that crack-induced debonding was crack length-dependent. The numerical fatigue life results were in good agreement with the experimental data when considering debonding and overestimated the experimental data without considering debonding, demonstrating the necessity of considering crack-induced debonding in calculation and design. Furthermore, a relationship was obtained between crack propagation and debonding development.

1. Introduction

Fatigue is one of the major concerns that may lead to sudden failure of steel structures and requires immediate repair. Fatigue failure generally occurs in steel structures subjected to cyclic loadings, leading to crack propagation and a final sudden rupture [1]. For cracked steel components, strengthening them is more economical and practical than replacing them. Compared with traditional strengthening methods, including stop holes, steel plate bolting and crack welding, the strengthening method that uses carbon fiber reinforced polymers (CFRPs) has been shown to be fast, convenient and efficient for cracked steel components [2–4]. This method adds very little weight and causes no damage to the original structure and can be widely used in strengthening steel structures under fatigue loadings. The fatigue behavior of cracked steel plates strengthened with CFRPs was studied experimentally and numerically [5–10], which found that fatigue life can be extended by up to 11.3 times that of unstrengthened specimens. Sharing the same strengthening mechanism, retrofitting damaged steel beams [11–14] and steel bridges [15,16] by externally bonding CFRPs to the lower flanges has been shown to be an efficient method under fatigue loadings. Furthermore, CFRPs can also be applied in strengthening steel joints under fatigue loadings [17]. Similarly, Guo et al. [18] studied the strengthening of rib-to-deck joints of orthotropic steel decks in steel bridges using externally bonded fiber-reinforced polymer (FRP) angles and found that the fatigue life-elongation ratio of the strengthened specimens reached 4.18 [18,19]. In addition, researchers have proposed using ultrahigh-modulus CFRPs [20] and prestressed CFRPs [21–23] to enhance fatigue behavior of steel members under fatigue loadings and found that the strengthening efficiency was more pronounced and that crack propagation could even be arrested.

When the externally bonded CFRP method is used in the strengthening of structures, the bond behavior between CFRP and steel is crucial for the strengthening efficiency and thus is widely considered. Many studies have been conducted to investigate the bond behavior of CFRP-steel interfaces by testing simple bonded joints. The bilinear and trapezoidal bond–slip relationships of the CFRP-steel bonded interfaces were observed, and bond–slip models were developed [32]. In addition,

* Corresponding author.
E-mail address: fengpeng@tsinghua.edu.cn (P. Feng).

https://doi.org/10.1016/j.tws.2021.108038
Received 4 November 2020; Received in revised form 21 April 2021; Accepted 31 May 2021
Available online 10 June 2021

Table 1
Previous studies on debonding of FRP-strengthened cracked metal plates [24–31].

Reference	Crack type	Debonding region from the tests
Lepretre et al. [33]	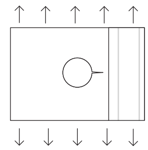 A center hole with a slot at one edge	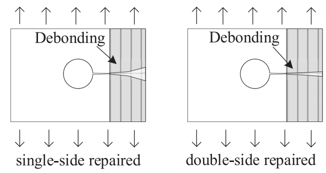 Cone shape for single-sided repair Trapezoidal shape for double-sided repair
Colombi et al. [34]	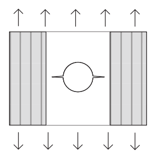 A center hole with two slots at two edges	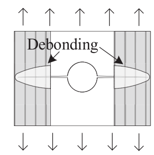 Elliptical shape
Mall and Conley [35], Zheng [36]	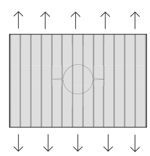 A center hole with two slots at two edges	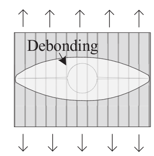 Elliptical shape
Hansen et al. [37]	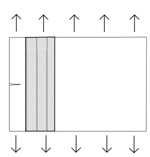 Single-edged crack	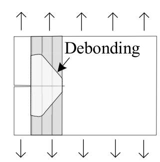
Zheng et al. [38]	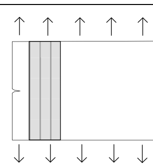 Single-edged crack	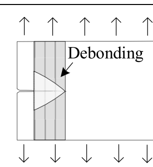
Baker. [39]	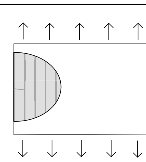 Single-edged crack	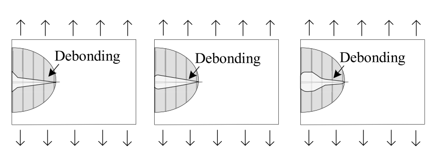 Either elliptical or wedge shape
Ye et al. [40]	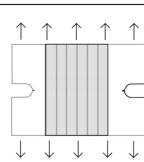 Double-edged crack	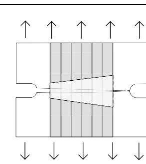 Approximately trapezoid shape

some studies investigated the effects of variable factors on the bond strength of CFRP-steel bonded interfaces, such as the steel surface preparation [33], environmental conditions (e.g., temperature, seawater exposure, humidity, UV light) [34], impact loading [34] and cyclic loading [35–37]. However, studies on the fatigue behavior of CFRP-steel interfaces remain rather limited [38]. A few studies have focused on evaluating the fatigue life and joint stiffness of bonded interfaces with double/single-bonded joints [38,39]. However, the simple bonded joints used in the previous studies are obviously different from CFRP-strengthened cracked steel members. Fatigue crack-induced debonding is more complicated and is one of the main failure modes of CFRP-strengthened cracked steel structures [40]. Some researchers [24–29] have observed or studied the crack-induced debonding of cracked metal plates strengthened with FRPs, as summarized in Table 1. Based on these studies [24–31,41], the debonding around the crack tip has a large influence on the crack propagation and fatigue life, so the CFRP efficiency reduction is a function of the debonding region area, which is influenced by the location and geometry of the initial crack and the location and configuration of the FRP. In addition, Bocciarelli et al. [42] analytically and numerically studied the debonding of a cracked steel beam strengthened with CFRPs, wherein the crack ran through the lower flange and the web. As the number of fatigue cycles increased, the crack propagated toward the depth of the web, but debonding developed in the interface of the lower steel flange and the CFRP, where the length of the crack was actually unchanged. This paper focuses on crack-induced debonding of a CFRP-strengthened tensile steel plate with a center hole with two slots at two edges, whose crack type is the same as that in [25–27]. For this crack type fully covered with CFRP, researchers [26,27] have found the debonding region to be an elliptical shape, however, to the best of the authors' knowledge, there are still no studies in the literature focusing on the relationship and interactions of the crack propagation and crack-induced debonding development, which are two interactional physical processes.

There are different methods for the prediction of fatigue life of the center-cracked tensile steel plate strengthened with CFRPs. First, the finite element method (FEM) is a commonly used technique for stress analysis, which can provide the stress intensity factor [7,8,14,18,19]. Similarly, the boundary element method (BEM) is another frequently used and well-established numerical technique that has been shown to be a convenient and accurate method for calculating the stress intensity factor and fatigue life [43,44]. In addition, linear elastic fracture mechanics (LEFM) is widely used to calculate the fatigue life, which is mainly based on the Paris law [5,6,14,45]. However, regarding these methods, there is very limited research on predicting fatigue life considering crack-induced debonding and its influence on the effectiveness of fatigue strengthening.

This paper experimentally and numerically studies the crack-induced debonding development and crack propagation in cracked steel plates strengthened by CFRP laminates and highlights the importance of considering the influence of crack-induced debonding in fatigue life predictions. In the following sections of this paper, "crack-induced debonding" is simply referred to as "debonding".

2. Interactional effects between crack propagation and debonding development

The mechanism of fatigue strengthening of cracked steel plates is complicated and includes crack propagation and debonding development processes, as shown in Fig. 1. For a pure cracked steel plate, the crack in the steel plate induces a stress concentration, which leads to crack propagation when the steel plate is under fatigue loading. When applying CFRPs to strengthen the steel plate, the CFRP deforms with the steel plate through the adhesive, sharing the tensile stress of the steel plate (especially around the crack tip), thus reducing the stress concentration/stress intensity factor at the crack tip and slowing the crack propagation. Therefore, the fatigue life of the steel plate is improved after strengthening.

However, in the crack propagation process, the stress concentration around the crack tip gradually increases, causing the deformation of the adhesive to increase. When the crack is sufficiently large, there will be a large stress concentration around the crack tip, thus the shear failure of the steel-adhesive interface will start, and debonding will be triggered around the crack tip. For normal-modulus CFRP-reinforced specimens, the process of the shear failure of the interface is mode II fatigue crack propagation of the interface, which requires the lowest fracture energy [24,28,30]. The occurrence of debonding affects the cooperative work between the CFRP and steel plate, weakening the reduction in stress concentration by the CFRP, thereby reducing the strengthening efficiency of the CFRP and leading to a higher stress concentration with a faster crack propagation rate than that without debonding in the next fatigue cycle. As the crack propagates in the next fatigue cycle, debonding develops; thus, its reduction in strengthening efficiency is more pronounced.

In summary, crack propagation and debonding development form an interactive and cyclic relation during the whole fatigue damage process of the CFRP-strengthened cracked steel plate. Crack propagation-induced debonding development affects the strengthening effectiveness of CFRPs, thereby influencing crack propagation in the next fatigue cycle. Therefore, the interactional effects between crack propagation and debonding development must be considered in fatigue life prediction and fatigue strengthening design. Otherwise, the fatigue life after strengthening will be overestimated, leading to unsafe results.

Table 2
Material properties of the steels.

Steel grade	Yield stress f_y (MPa)	Ultimate tensile strength (MPa)	Thickness (mm)
Q345D	390	509	16
Q460C	481	612	12
Q690D	805	823	14

3. Fatigue tests with debonding measurements

3.1. Material

In the fatigue test, Q345, Q460 and Q690 steel are used, and their material properties are shown in Table 2. The elastic modulus E_s and Poisson's ratio γ of all steels are 201 GPa and 0.3, respectively. The CFRP laminate, provided by HS Co., Ltd. (Jiangsu Province, China), has an ultimate tensile strength f_P of 2454 MPa, an elastic modulus E_P of 168 GPa and Poisson's ratio γ of 0.3. As suggested by the manufacturer, the adhesive Araldite-2015 is used with the CFRP laminate. By standard measurements [46], as shown in Fig. 2, the elastic modulus E_a and ultimate strength f_a of the adhesive are 2.10 GPa and 23.5 MPa, respectively.

3.2. Specimen and test setup

The specimen configuration is presented in Fig. 3(a), which is consistent with those used in previous studies [45,47,48]. The rectangular steel plate has a length of 400 mm, a width of 70 mm and a thickness of 12 mm, 14 or 16 mm. The steel plate is cracked by wire-electrode cutting before testing. The depth of the crack is the same as that of the steel plate. The CFRP laminates are applied on both sides of the steel plates, each of which has a length of 200 mm, a width of 50 mm and a thickness of 1.4 mm.

The specimen preparation is as follows: (1) The steel plate surface was sandblasted and then cleaned with acetone to obtain a rough and clean surface. (2) Then, the adhesive was uniformly distributed on the steel and CFRP surfaces. The CFRP laminates were pressed on the steel substrate immediately after the surface preparation [6]. (3) Then, to avoid end-debonding of the CFRP laminate, a 50 mm wide CFRP sheet was wrapped around the end of the CFRP laminates. (4) Finally, a vacuum curing process and a weight plate were applied to the specimens to achieve a uniform bond layer by the three-dimensional pressure environment for one-week of curing, as shown in Fig. 3(b). With this method, the adhesive thickness of the strengthened specimens was maintained at 0.5 mm.

To study the debonding of the CFRPs and steel under a high stress range, three CFRP laminate-strengthened specimens (LS) and three unstrengthened reference specimens (U) with the same stress level (defined as the ratio of maximum stress in the fatigue loading σ_{max} to the yield stress f_y) of 50% were investigated, as shown in Table 3. The subscripts 345, 460, or 690 denote the steel grade, followed by σ_{max}. The stress ratio R is 0.1 for the base loading cycles; the stress ratio is

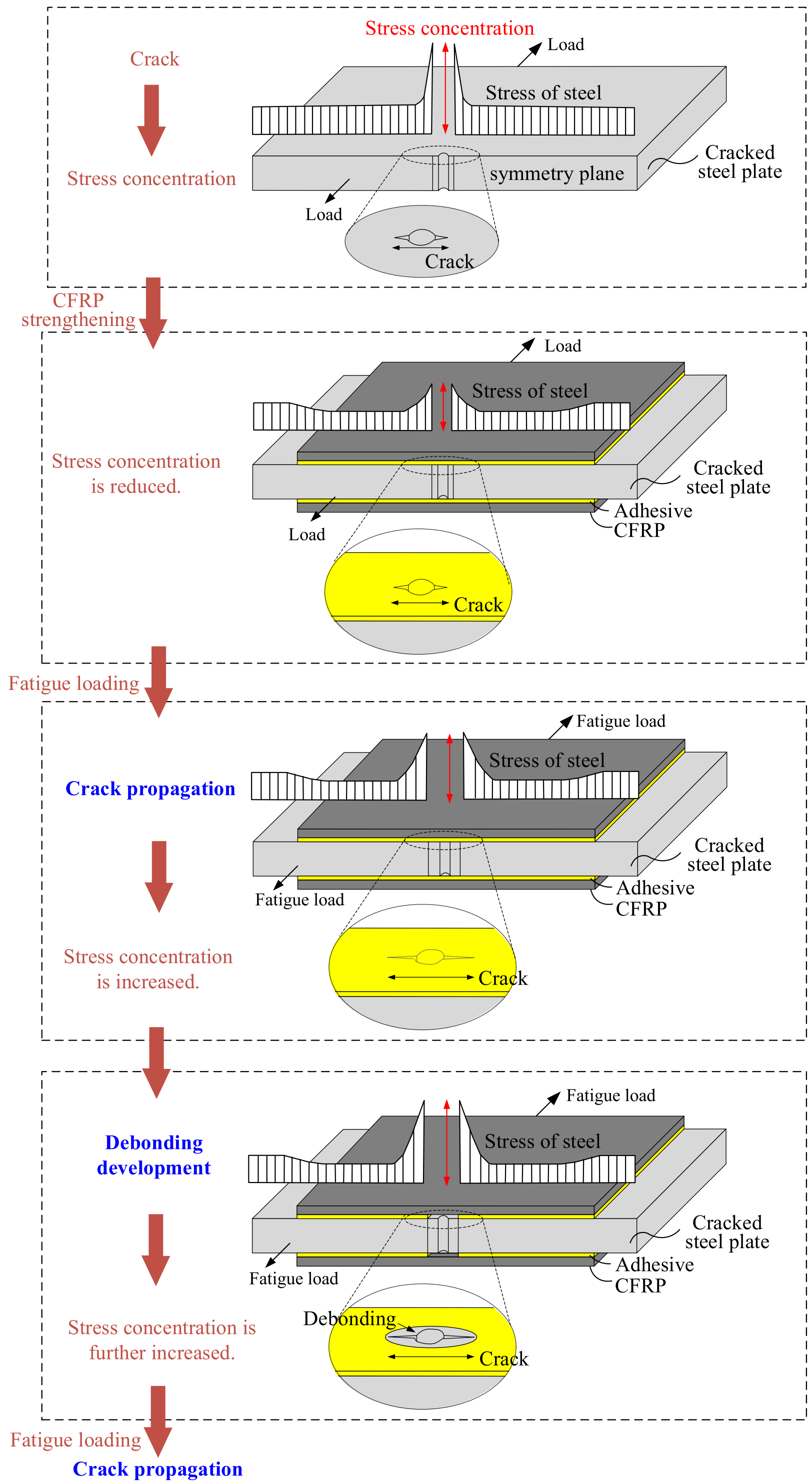

Fig. 1. Interactional effects between crack propagation and debonding development.

0.6 for the marking loading cycles to track crack propagation by the beach marking method [2]. The loading sequences of all specimens are shown in Appendix. The marking loading cycles will not be included in the fatigue cycles because of their small stress range [2]. The fatigue frequency is kept as 5 Hz for most specimens. For U690-402.5 and SL690-402.5, because the maximum force is 394.5 kN, which is approximately 80% of the maximum loading of the loading machine (i.e., 500 kN), the frequency is reduced from 5 to 3 Hz in order to ensure the safety of the loading machine. Based on reference [27], frequencies between 200 and 700 times/min (3.33 and 11.67 Hz) have little effect on fatigue strength.

Although debonding at the CFRP-steel interface cannot be visually detected, the debonding region can be obtained by the strain gradient of the CFRP laminate. Thus, for the strengthened specimens, the noncontact strain acquisition method called digital image correlation (DIC) is used to measure the longitudinal strain of the CFRP laminate surface during fatigue loading [49], as shown in Fig. 3(c). This process is achieved by a three-dimensional optical strain measurement system (i.e., ARAMIS 3D) including a cold light source, two charge coupled

Table 3
Details of the fatigue tests.

Specimen	Form	f_y (MPa)	σ_{max} (MPa)	σ_{max}/f_y	Stress range $\Delta\sigma$ (MPa)	Frequency (Hz)
U345-195.0	Unstrengthened	390	195		175.5	5
SL345-195.0	Strengthened	390	195		175.5	5
U460-240.5	Unstrengthened	481	240.5	50%	216.5	5
SL460-240.5	Strengthened	481	240.5		216.5	5
U690-402.5	Unstrengthened	805	402.5		362.3	3
SL690-402.5	Strengthened	805	402.5		362.3	3

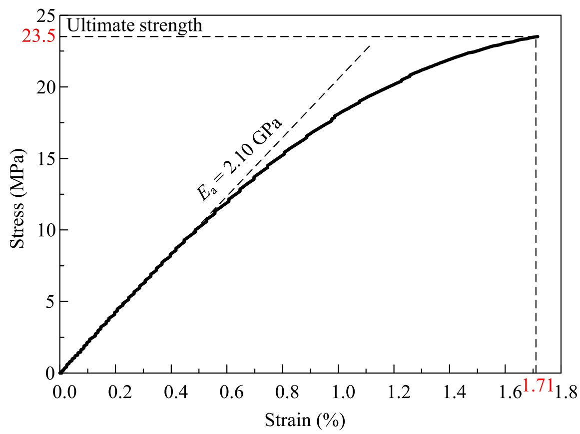

Fig. 2. Stress–strain curve of adhesive Araldite-2015.

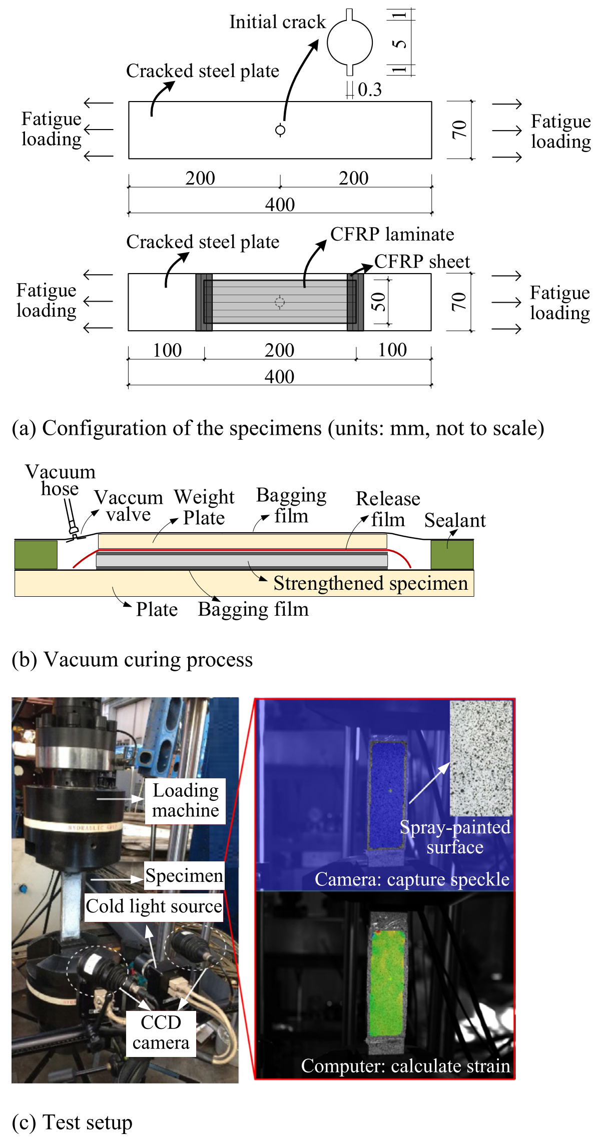

Fig. 3. Specimen and test setup.

device (CCD) cameras and a computer equipped with DIC algorithm software. The following steps are conducted: (1) Apply the base loading cycles, and then apply marking loading cycles so that the crack length can be obtained. (2) Increase the load to reach the maximum stress of the base loading cycles, and then capture the strain distribution of the CFRP laminate by DIC, from which the strain gradient distribution along the longitudinal direction of the CFRP laminate can be obtained. (3) Repeat the above steps until the specimen fails by fracture. The time of capturing the strain distribution by DIC is shown in Fig. 4(a).

3.3. Test results and analysis

3.3.1. Fatigue life and crack propagation

The crack length vs. fatigue cycle curves obtained by the beach marking method are shown in Fig. 4. The beach marking method is effective because clear beach marks are left on the fracture surface of the specimen, by which it is found that the crack development is slow at the beginning, and gradually becomes fast, rapidly followed by a sudden fracture in the end. For Q690 steel, crack propagation is very fast under the high stress range applied.

The fatigue life results are summarized in Fig. 5(a). Compared with the results of the same unstrengthened specimens in the literature [6], at the same stress level (50%), the strengthening provided by the CFRP laminates is effective, increasing the fatigue life by factors of 1.53 to 3.84. In addition, a typical failure mode is shown in Fig. 5(b), in which it is clear that debonding occurred around the crack tip.

3.3.2. Debonding region

The strain distributions of the CFRP laminates of the three specimens acquired by DIC are shown in Fig. 6. In general, when the crack is small, the strain distribution on the surface of the CFRP laminate is relatively uniform, whereas when it reaches a long length, strain concentration occurs near the crack. Taking specimen SL460-240.5 as an example, the CFRP strain distribution is basically uniform before 120,000 fatigue cycles. Afterward, the CFRP around the initial crack begins to exhibit strain concentration. At this stage, as the fatigue crack propagates, the strain concentration area expands relatively slowly. Starting from approximately 250,000 fatigue cycles, the strain concentration area increases rapidly with increasing fatigue cycles.

Because of the central crack, which is an initial damage to the steel plate, there is a stress concentration around the crack. Thus, the CFRP strain is very large, making the CFRP strain gradient large. Because the adhesive shear stress is proportional to the strain gradient of the CFRP laminate [29], a large strain gradient of CFRP means a high shear stress of adhesive, so at this time, the debonding occurs. When the crack propagates, this high strain region expands, so debonding develops.

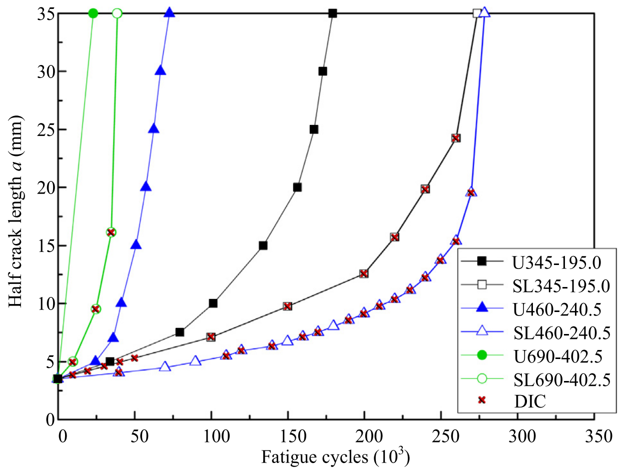

(a) Crack length vs. fatigue cycle curves

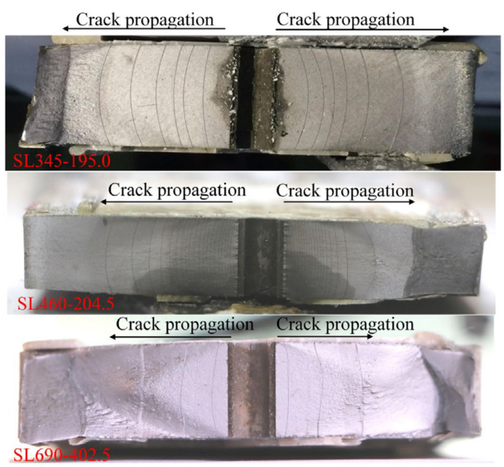

(b) Beach marking results

Fig. 4. Crack length vs. fatigue cycle curves by the beach marking method.

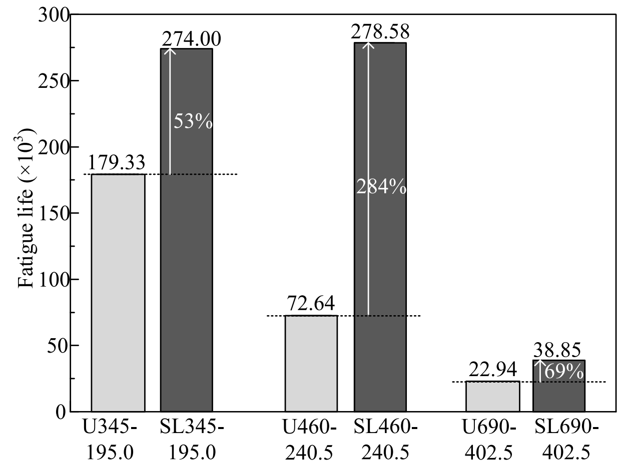

(a) Fatigue life

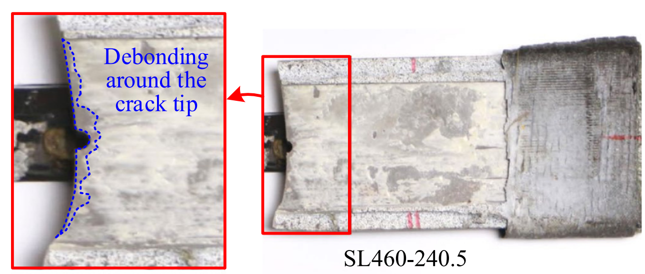

(b) Typical failure mode

Fig. 5. Fatigue life and failure mode.

The following method is used to determine the debonding region: because the shear stress is transferred outside the debonding region and no shear stress can be transferred inside the debonding region, the debonding region edge is a contour of high CFRP strain gradient, and the debonding region is bounded by this contour which has negligible CFRP strain gradient [29]. Therefore, based on the DIC results, the strain gradient of the CFRP laminates is studied. Specifically, as shown in Fig. 7, the Y-coordinate of point i is y_i, and the strain in the y direction at this point is $\varepsilon_{y,i}$; the point above it is named point i+1, for which the Y-coordinate is y_{i+1} and the strain in the y direction is $\varepsilon_{y,i+1}$. Eq. (1) can be used to obtain the strain gradient in the y direction $d_{\varepsilon,i}$ of point i. By using the same method, the strain gradients of all points in the CFRP laminates are obtained. The "Griddata" interpolation function in MATLAB [50] is used to draw the graph of the debonding region by DIC. A strain gradient higher than 0.06 με/m is considered the debonding region edge, and the region enclosed by the edge contour is considered the debonding region. The results of the debonding regions will be shown and analyzed in comparison to the BEM results in Section 4.3.1.

$$d_{\varepsilon,i} = (\varepsilon_{y,i+1} - \varepsilon_{y,i})/(y_{i+1} - y_i) \tag{1}$$

4. Simulation by the BEM

To study the influence of debonding on the fatigue life and the relationship between crack propagation and debonding development, the cracked steel plates strengthened by CFRP laminates (specimens SL345-195.0, SL460-240.5 and SL690-402.5) are analyzed by the BEM in this section.

4.1. Introduction of the BEM

In practical engineering, only a few cases can be solved by analytical methods. With the development and popularization of computer technology, numerical methods have gradually become an effective method to solve boundary value problems. Numerical solutions can be divided into regional and boundary types. The regional numerical methods mainly include the FEM and the finite difference method, and the boundary numerical method is mainly BEM.

The BEM is a new numerical analysis method developed after the FEM in the 1970 s [51], which solves boundary integral equations. Compared with the FEM, the BEM has the following advantages: the BEM establishes and divides elements only for the boundaries of a solid model, so it reduces the number of elements and degrees of freedom and maintains a high calculation precision, which is especially suitable for analyzing fracture problems with singular stresses [52]. In addition, when it is used to simulate a crack propagation process, the remeshing of the crack tip can be accomplished automatically, and the fatigue life

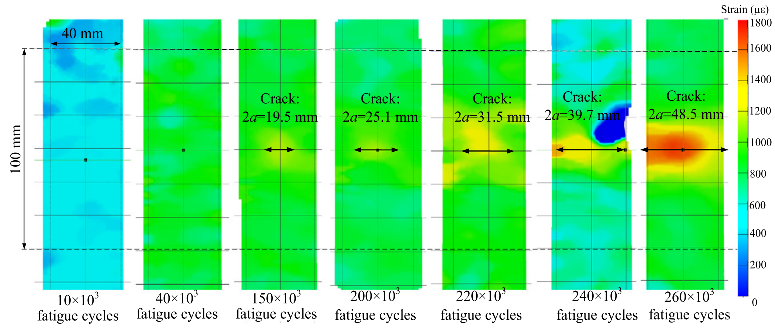

(a) SL345-195.0 (the blue area in the second-to-last graph is caused by the unsmooth surface of the CFRP)

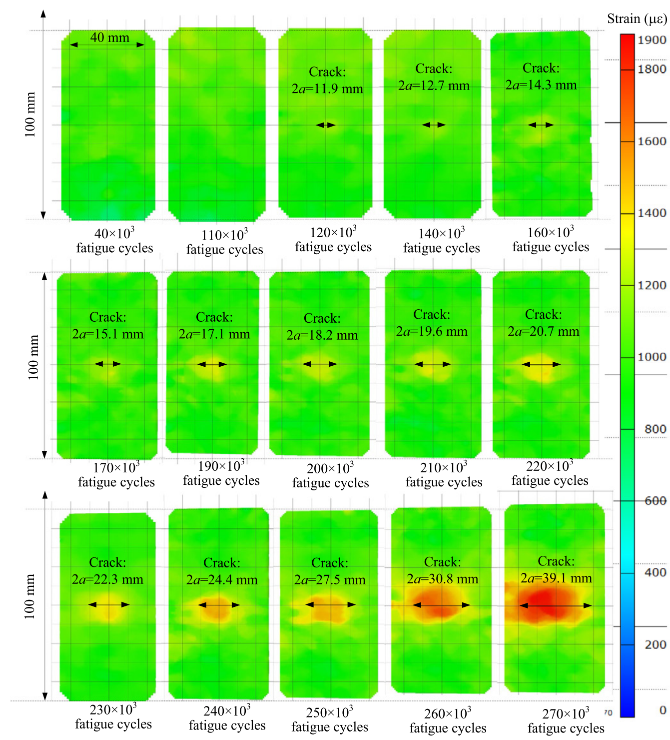

(b) SL460-240.5

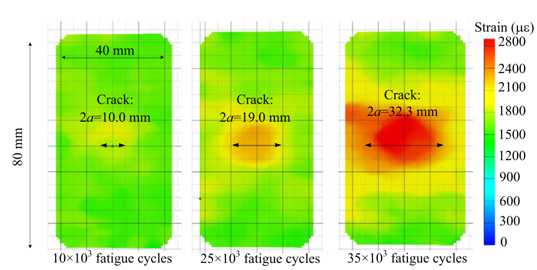

(c) SL690-402.5

Fig. 6. CFRP strain distributions acquired by DIC.

can be obtained directly. Therefore, the BEM is a powerful alternative to the FEM for problems involving cracks [43,44,53].

The computer program BEASY can be applied to perform numerical analyzes based on the BEM; this software is an internationally recognized leader in computer simulations for defect assessment and crack propagation [54]. Thus, it is used in this paper for simulation.

4.2. Modeling

4.2.1. Geometry configurations and elements

For each specimen, the steel plate with a central round hole and the CFRP laminate were modeled three dimensionally according to real dimensions in the tests. Due to the symmetry of the geometry and boundary conditions, only half of the specimen, which is symmetric

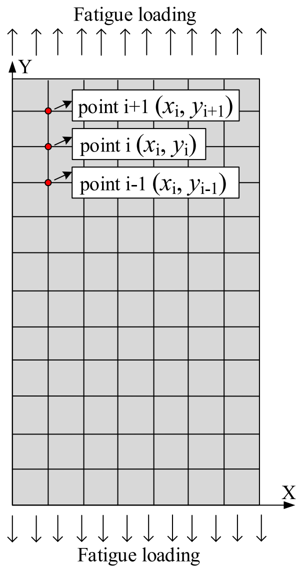

Fig. 7. Schematic diagram of the calculation of the CFRP strain gradient in the loading direction.

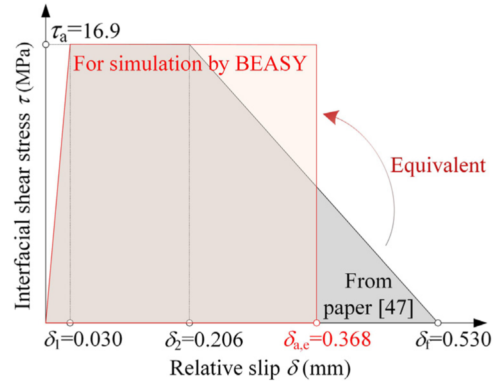

Fig. 9. Bond–slip relationship of Araldite-2015 adhesive and its equivalent one in BEASY [56].

with respect to the Y–Z plane, was modeled and meshed. Fig. 8 shows a typical specimen configuration and details of the initial crack in BEASY based on Section 3.

To ensure the accuracy and efficiency of the calculations, the steel plate and CFRP laminate were modeled as continuous plates by Q38 elements, which are quadrilateral, reduced quadratic order elements. The dimensions of Q38 element are 5 mm × 5 mm. A relatively fine mesh was adopted in the area around the center hole due to the existence of a high stress concentration. The element size around the center hole was less than 1/4 of that in the other areas [43]. The above meshing has been verified to be sufficiently fine [55].

According to the test, a debonding region occurred around the crack tips. Therefore, the steel plate and CFRP cannot be tied together. Thus, the adhesive used to bond the CFRP to the steel plates was modeled as continuously distributed springs connecting the CFRP and the steel plate, considering three directions, as shown in Fig. 8.

Because BEASY only provides elastic elements, the local yielding zone of the crack tip has not been considered. In addition, elastic springs are used, under which situation a method is proposed in Section 4.2.2 to consider debonding.

4.2.2. Material properties and consideration of debonding

The material properties of the steel and CFRP in the BEM are from the test results in Section 3.1. The spring stiffness is defined in terms of normal and tangential directions in a local coordinate system. K_t and K_u are the in-plane stiffness of the spring, and K_n is the out-of-plane stiffness of the spring. K_X, K_Y, K_Z denote the stiffness of the spring in the X, Y, Z directions, respectively.

For the out-of-plane springs, the stiffness value, specified in units of MPa/mm, can be obtained by Eq. (2) [44,54], where t_a is the adhesive thickness, equal to 0.5 mm according to measurements. Thus, K_Z is 4200 MPa/mm.

For the springs in the X–Y plane, an equivalent bond–slip relationship of the CFRP-steel interface, bonded with an Araldite-2015 adhesive layer of 0.5 mm thickness, is proposed based on the results from a previous study using the same adhesive of the same thickness [56], as shown in Fig. 9. For the bond–slip relationship from reference [56], τ_a is the shear strength, and δ_1, δ_2 and δ_f are three parameters of the relative slip. The energy release rate is an important parameter for the interfacial bond behavior [32], which is the area below the bond–slip curve. Thus, the equivalent bond–slip is proposed by keeping the energy release rate the same. Specifically, $\delta_{a,e}$ is used, which is the average value of δ_2 and δ_f. If the energy release rate threshold is reached, debonding occurs. The following steps are conducted to achieve this goal using the elastic springs and the equivalent bond–slip relationship. First, spring stiffnesses K_X and K_Y can be obtained by Eq. (3). Second, after an incremental step of crack propagation, the stresses of all springs in all directions are checked. For the springs whose stress reaches the shear strength τ_a and the deformation reaches δ_1, their stiffness is reduced to zero, but the stress is kept at the shear strength τ_a; for the springs whose deformation reaches $\delta_{a,e}$, they are deleted because debonding is assumed to occur. Then, the above steps are repeated in the next incremental steps until complete failure is reached.

$$K_Z = K_n = \frac{E_a}{t_a} \tag{2}$$

$$K_X = K_Y = K_t = K_u = \frac{\tau_a}{\delta_1} \tag{3}$$

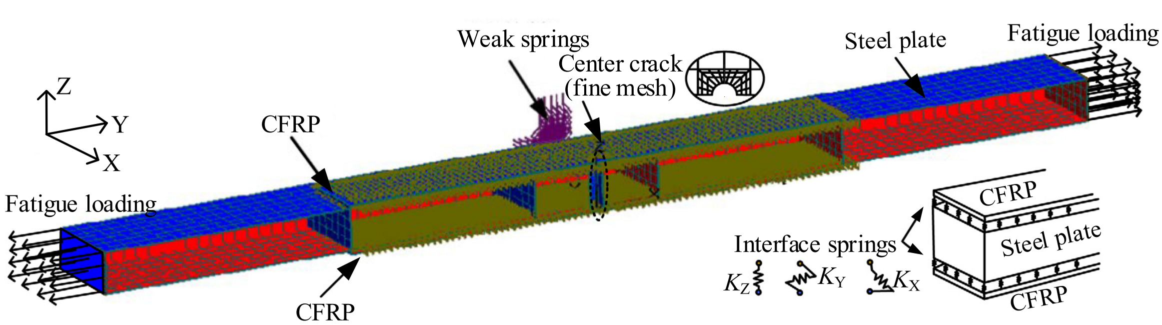

Fig. 8. Boundary element model in BEASY.

4.2.3. Boundary conditions

All models were subjected to a uniform amplitude tensile cyclic loading according to the real test data in Table 3. Weak springs over the middle elements along the length of the steel plate were added to provide a rigid body restraint [54]. The stiffness of the weak springs was set as 10% of the elastic modulus of the steel (i.e., 20.1 GPa) for the three directions.

4.2.4. Crack growth law and fatigue parameters

The type of crack, crack growth law and fatigue parameters were defined in BEASY Fracture Wizard.

(1) Definition of crack

First, the crack type is defined as “through-crack” with a depth equal to the thickness of the steel plate. The initial crack length is 7 mm. With the increase in fatigue cycles, the initial crack at the central hole along the width of the steel plate spreads along the width, which is perpendicular to the loading direction. Thus, to reduce the calculation time of the fatigue crack growth, remeshing of the elements is carried out only in the region around the crack tip along the width of the steel plate. The remeshing size of the elements has minimum and maximum limits. The minimum remeshing size recommended by BEASY is 10% of the through-crack thickness [54]. In this paper, the minimum remeshing size is set as 0.5 mm, and the maximum remeshing size is set as 2.5 mm.

(2) Definition of the crack growth law

In this study, considering the influence of the plastic zone of the crack tip, the NASGRO 3 law [57] is adopted as the crack growth law as expressed in Eqs. (4)–(6).

$$\frac{da}{dN} = \frac{C\cdot(1-f)^n\cdot\Delta K^n\cdot\left(1-\frac{\Delta K_{th}}{\Delta K}\right)^p}{(1-R)^n\cdot\left[1-\frac{\Delta K}{(1-R)\cdot K_c}\right]^q} \tag{4}$$

$$f = \begin{cases} \max(R, A_0 + A_1R + A_2R^2 + A_3R^3) & R \geq 0 \\ A_0 + A_1R & -2 \leq R < 0 \end{cases} \tag{5}$$

$$\begin{cases} A_0 = (0.825 - 0.34\alpha + 0.05\alpha^2)\cdot\left[\cos\left(\frac{\pi}{2}\cdot\frac{\sigma_{max}}{\sigma_0}\right)\right]^{1/\alpha} \\ A_1 = (0.415 - 0.071\alpha)\cdot\frac{\sigma_{max}}{\sigma_0} \\ A_2 = 1 - A_0 - A_1 - A_3 \\ A_3 = 2A_0 + A_1 - 1 \end{cases} \tag{6}$$

$$\frac{da}{dN} = C\cdot(\Delta K)^n \tag{7}$$

In Eq. (4), N is the number of fatigue cycles; a is the half crack length; R is the stress ratio; ΔK is the range of the stress intensity factor; and C, n, p, q are empirical constants. Moreover, f is the crack opening function, which is introduced to consider the effect of crack closure induced by the plastic zone of the crack tip on the crack growth rate [58]. This function is determined by R; the plane stress–strain factor α; the flow stress σ_0, which is the average between the uniaxial yield stress and ultimate tensile strength of the material; and the maximum stress in fatigue loading σ_{max}, as shown in Eqs. (5) and (6). K_c is the critical stress intensity factor range. ΔK_{th} is the threshold stress intensity factor range. When crack closure induced by the plastic zone of the crack tip is not considered, the empirical constants $p = q = 0$ and $f = R$ when R is between 0 and 1. Then, the NASGRO 3 law is simplified as the Paris law [5–7], as shown in Eq. (7).

The cracks will propagate automatically in BEASY until the range of the stress intensity factor ΔK is greater than K_c or the crack propagation size of the last incremental step is larger than the remaining size of the specimen in the crack propagation direction when complete failure is reached.

(3) Fatigue parameters

The material properties of the steel plate were first selected from the predefined database whose yield strength and ultimate strength were closest to the test results. Thus, p, q and K_c are obtained. However, regarding the fatigue parameters C and n related to the material, although these parameters are provided for nearly 100 kinds of ferro-containing alloys in the NASGRO database, those of the normal and high-strength steels in this paper, which were made in China, must be studied. Specifically, based on the crack propagation data of unstrengthened steel plates from a previous study [7], a relationship between a and N is fitted as shown in Eq. (8). Based on the calculation of ΔK by BS7910-2005 [59] (Eq. (9)), where W is the width of the steel plate, the relationship between ΔK and a for the specimens in this paper is fitted as shown in Eq. (10).

Table 4
Fatigue parameters of the specimens in BEASY.

Specimen	C	n	p	q	K_c (MPa · mm$^{1/2}$)
U345-195.0 SL345-195.0	5.24×10^{-9}	1.46	0.5	0.5	4170
U460-240.5 SL460-240.5	1.92×10^{-9}	1.62	0.5	0.5	6950
U690-402.5 SL690-402.5	8.32×10^{-11}	2.03	0.25	0.25	9730

$$N = -101153 + 35719a - 2006a^2 + 53.83a^3 - 0.547a^4 \tag{8}$$

$$\Delta K = Y\cdot\Delta\sigma\cdot\sqrt{\pi a} = \sqrt{\sec\left(\frac{\pi a}{W}\right)}\cdot\Delta\sigma\cdot\sqrt{\pi a} \tag{9}$$

$$\Delta K = 888.1093 - 144.8374a + 27.9456a^2 - 1.4654a^3 + 0.0268a^4 \tag{10}$$

In addition, the ΔK_{th} value adopted is 148.6 MPa mm$^{1/2}$ according to Eq. (11) [59,60] when R is 0.1. σ_{max}/σ_0 can be calculated by the data in Table 3. α is determined from BEASY. Thus, f can be obtained. For example, for U345-195.0 and SL345-195.0, $\sigma_{max}/\sigma_0 = 0.3$, $\alpha = 2.5$, and $f = 0.292$.

$$\Delta K_{th} = \begin{cases} 63 & R \geq 0.5 \\ 170 - 214R & 0 \leq R < 0.5 \\ 170 & R < 0 \end{cases} \tag{11}$$

Substituting the above results into Eq. (4) results in Eq. (12). Finally, the least-squares method is used to evaluate the best fit for parameters C and n, and the results are shown in Table 4.

$$\ln\frac{da}{dN} = \ln C + n\cdot\ln(0.8\Delta K) + 0.5\ln\left(1-\frac{148.6}{\Delta K}\right) - 0.5\ln\left(1-\frac{\Delta K}{3753}\right) \tag{12}$$

4.3. Simulation results

4.3.1. Debonding region

The debonding region measured by DIC from Section 3.3 is compared with that simulated by the BEM with the same fatigue crack length. For specimens SL345-195.0 and SL690-402.5, as shown in Fig. 10(a) and (c), the shapes and areas of the debonding regions simulated by the BEM are very similar to those obtained by DIC. For specimen SL460-240.5, as shown in Fig. 10(b), the shapes of the debonding regions by the BEM and DIC are similar, while the area of the debonding region determined by the BEM is smaller than that determined by DIC, which is due to the fatigue test discreteness and DIC measurement error.

4.3.2. Fatigue life

With or without considering the influence of debonding, the fatigue lives of the six specimens predicted by the BEM are shown in Table 5. N_t is the fatigue life from the tests in Section 3, N_{BEM} is the fatigue life determined by the BEM without considering debonding, and $N_{BEM,d}$ is the fatigue life determined by the BEM considering debonding. The crack length vs. fatigue life curves from the tests and by the BEM

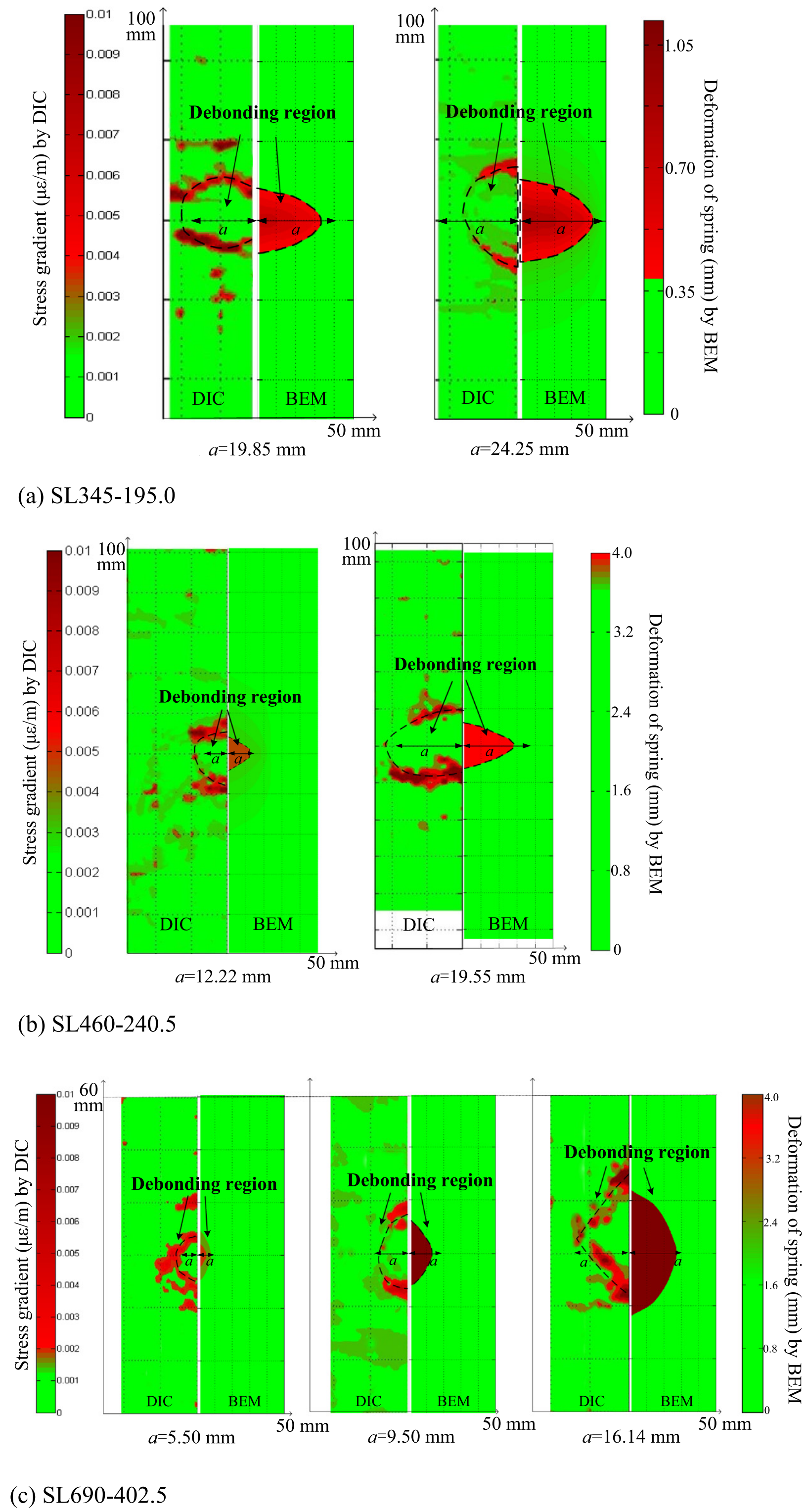

Fig. 10. Comparison of the debonding region determined by DIC and the BEM.

considering debonding are compared in Fig. 11, and the fatigue lives N_t, N_{BEM} and $N_{BEM,d}$ are compared in Fig. 12.

Except for specimen SL460-240.5, $N_{BEM,d}$ gives a good prediction of the test fatigue life N_t; the value of $N_{BEM,d}/N_t$ ranges from 0.95 to 1.18, and the average value is 1.06. While, N_{BEM} overestimates the test fatigue life N_t of strengthened specimens by 54% to 84%, which is extremely unsafe in fatigue design. The result that SL460-240.5 has a much longer test fatigue life compared with the fatigue life determined by the BEM may be attributed to its noncontinuous fatigue loading procedure, which was stopped three times due to problems with the test machine.

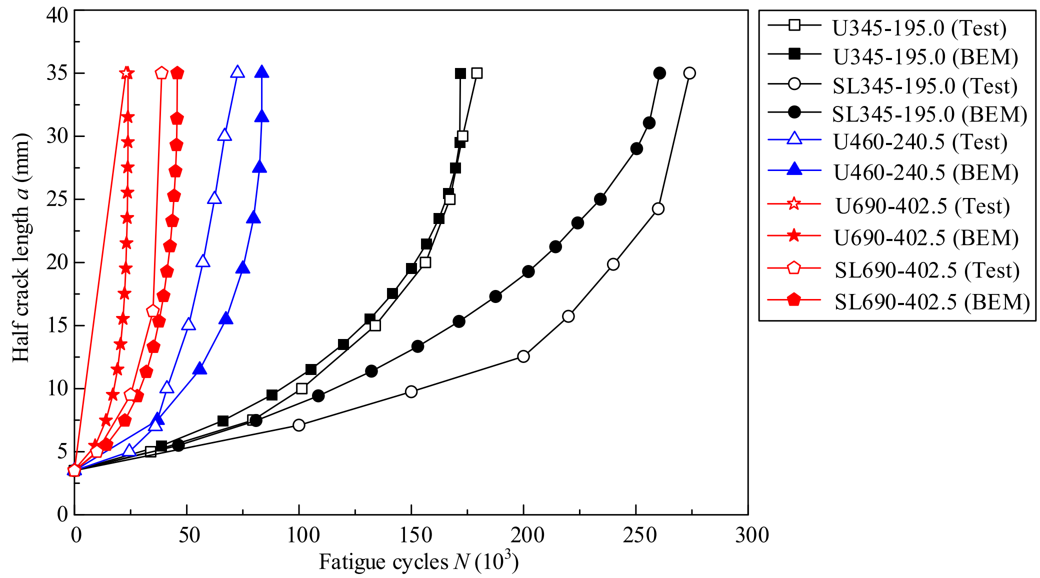

Fig. 11. Comparison of the crack length vs. fatigue life curves from the tests and the BEM considering debonding.

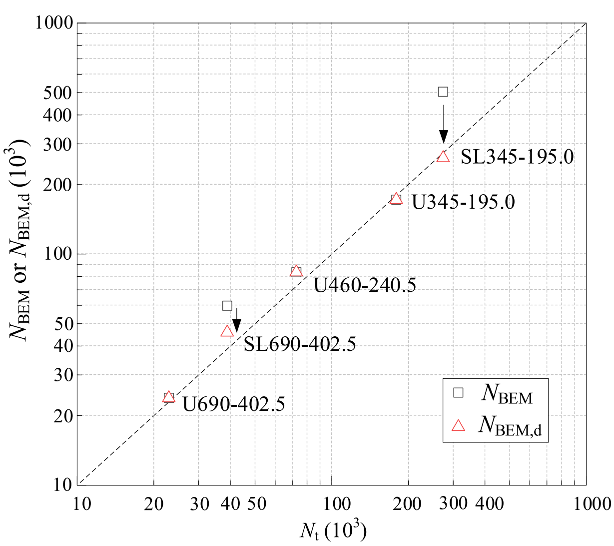

Fig. 12. Comparison of fatigue lives from the tests and the BEM with and without considering debonding.

Table 5
Fatigue lives of the specimens from tests and the BEM.

Specimen	N_t (10^3)	N_{BEM} (10^3)	$N_{BEM,d}$ (10^3)	N_{BEM}/N_t	$N_{BEM,d}/N_t$
U345-195.0	179.33	171.88	171.88	0.96	0.96
SL345-195.0	274.00	503.70	260.64	1.84	0.95
U460-240.5	72.64	83.47	83.47	1.15	1.15
SL460-240.5	278.58	155.96	–	Fail	Fail
U690-402.5	22.94	23.83	23.83	1.04	1.04
SL690-402.5	38.85	59.71	45.85	1.54	1.18

4.3.3. Relationship between crack propagation and debonding development

The stresses of the interface springs can be extracted from the BEASY result files in every incremental step of crack propagation. Thus, an accurate relationship between crack propagation and debonding development is obtained. Taking specimens SL345-195.0 and SL690-402.5 for example, which were successfully simulated in Section 4.3.2, the results are shown in Fig. 13. The half crack length is a, and the length of the debonding region along the direction of crack propagation is defined as a_d. Point A in Fig. 13 represents the starting time of debonding along the crack propagation direction, point B represents the time when the debonding develops to the edge of the CFRP laminate, and point C represents the end of debonding development.

From point A to point B, the debonding development law of the two specimens is basically similar. In this period, debonding develops along the direction of crack propagation and in the direction perpendicular to crack propagation. The debonding development rate along the crack propagation direction is very similar to the crack propagation rate most of the time, and the length of the debonding region in the direction perpendicular to the crack propagation is approximately 1/5 of a_d, which is in accordance with reference [25]. The difference between the two specimens is as follows: (1) For specimen SL345-195.0, debonding starts when a is 11.4 mm, whereas for SL690-402.5, debonding starts when a is only 6.5 mm. (2) For specimen SL345-195.0, $a > a_d$. However, for specimen SL690-402.5, a is larger than a_d at the beginning, but when a is 19.5 mm, a_d reaches 23.9 mm, and the state of $a < a_d$ is maintained for a period until debonding develops to the edge of the CFRP laminate. This difference can be summarized as follows: with the increase in the fatigue stress range $\Delta\sigma$, the start of debonding occurs earlier, and a_d increases faster, which can reach and even surpass a. This finding can be explained as follows: with the increase in the fatigue stress range, the shear stress in the adhesive increases, and because the debonding is governed by shear failure and mode II crack propagation of the interface [24,28,30], a larger area of debonding occurs for the same crack length.

From point B to point C, since the crack length exceeds the coverage of the CFRP laminate, the debonding no longer develops along the crack propagation direction and develops only in the direction perpendicular to the crack propagation until the failure of the specimen.

5. Conclusions

This paper presents an experimental and numerical investigation on the crack propagation and debonding development in cracked steel plates strengthened by CFRP laminates under different stress ranges, from which the following conclusions are drawn:

(1) Crack propagation and debonding development form an interactive and cyclic relation during the whole fatigue damage process of the CFRP-strengthened cracked steel plate. Debonding initiation and development are affected by fatigue stress range, crack length, stiffness of CFRP and steel plate, steel grade, etc.

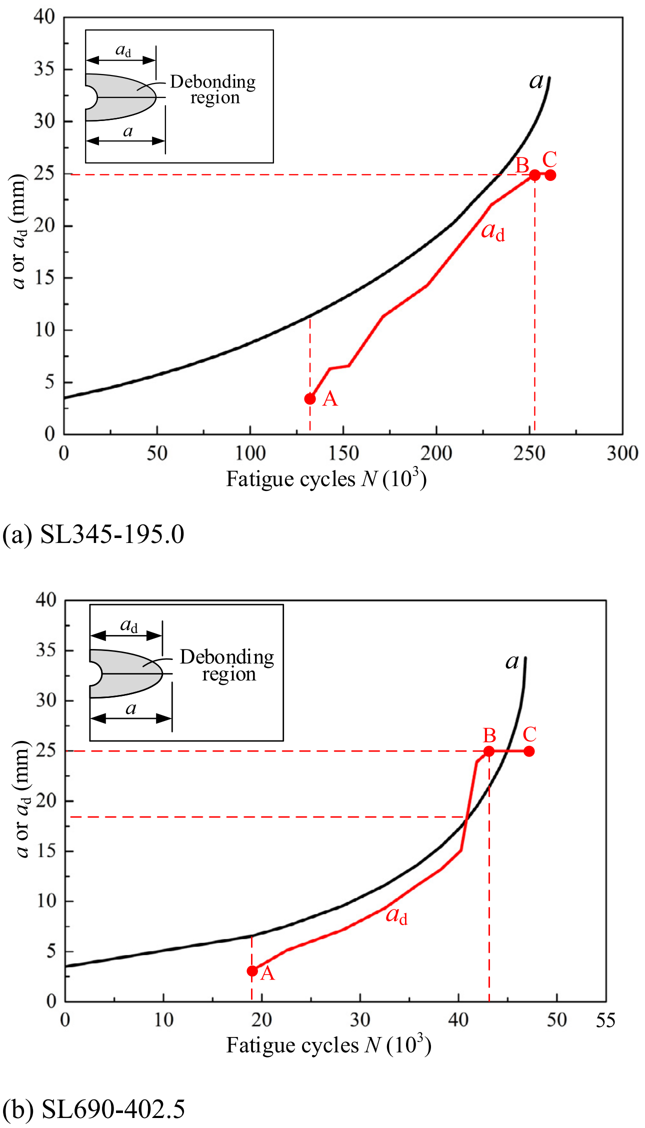

Fig. 13. Relationship between crack propagation and debonding development determined by the BEM.

(2) The experimental results show that the debonding region can be obtained by calculating the strain gradient distribution of the CFRP laminate by the strain distribution of the CFRP laminate by means of the DIC technique.

(3) There is good agreement between the numerical and experimental results, which demonstrates that the BEM can be successfully used for accurately estimating the fatigue behavior of CFRP laminate-strengthened steel plates considering debonding.

(4) Debonding of the CFRP around the crack tip reduces the strengthening efficiency of the CFRP. Thus, considering debonding is necessary for simulating and designing CFRP laminate-strengthened steel plates under fatigue loadings. Otherwise, the predicted fatigue life will be overestimated, leading to unsafe results.

(5) Debonding of the CFRP around the crack tip develops with crack propagation under fatigue loading. Initially, debonding develops along and perpendicular to the crack propagation direction. In this period, the debonding development rate along the crack propagation direction is very similar to the crack propagation rate most of the time. For the specimen under a small stress range, debonding occurs late, and the debonding length a_d is smaller than the crack length a, whereas for the specimen under a large stress range, debonding occurs early, and a_d can reach and even surpass a. Then, since the crack length exceeds the coverage of the CFRP, the debonding develops only perpendicular to the crack propagation direction until the failure of the specimen.

CRediT authorship contribution statement

Lili Hu: Methodology, Investigation, Data curation, Visualization, Writing - original draft, Writing - review & editing. **Yuanyuan Wang:** Formal analysis, Investigation, Visualization, Software, Validation. **Peng Feng:** Conceptualization, Methodology, Supervision, Project administration, Funding acquisition, Validation, Writing - review & editing. **HaiTao Wang:** Validation, Writing - review & editing. **Hanlin Qiang:** Data curation, Visualization.

Declaration of competing interest

The authors declare that they have no known competing financial interests or personal relationships that could have appeared to influence the work reported in this paper.

Data availability

All data, models, and code generated or used during the study appear in the submitted article.

Acknowledgments

This work was financially supported by the National Key Research and Development Program of China (No. 2017YFC0703001), the National Natural Science Foundation of China (No. 51578559 and No. 51708174), Shanghai Sailing Program (No. 21YF1419500) and start-up funding provided by Shanghai Jiao Tong University.

Appendix. Loading sequences of specimens

Specimen	Loading type	Fatigue cycles	Repeating times
U345-195.0	Base loading Marking loading	30,000 15,000	5 times
	Base loading	29,330	1 time
	Fatigue cycles of base loading: 179,330; Total fatigue cycles: 254,330		
U460-240.5	Base loading Marking loading	30,000 15,000	2 times
	Base loading	12,640	1 time
	Fatigue cycles of base loading: 72,640; Total fatigue cycles: 102,640		
U690-402.5	Base loading	22,940	1 time
	Fatigue cycles of base loading: 22,940; Total fatigue cycles: 22,940		
SL345-195.0	Base loading Marking loading	10,000 5,000	5 times
	Base loading Marking loading	50,000 5,000	3 times
	Base loading Marking loading	20,000 5,000	3 time
	Base loading	14,000	1 time
	Fatigue cycles of base loading: 274,000; Total fatigue cycles: 329,000		
SL460-240.5	Base loading Marking loading	40,000 10,000	1 time
	Base loading Marking loading	30,000 10,000	1 time
	Base loading Marking loading	20,000 5,000	2 times
	Base loading Marking loading	10,000 5,000	1 time
	Base loading Marking loading	20,000 5,000	1 time
	Base loading Marking loading	10,000 5,000	5 times
	Base loading Marking loading	10,000 3,000	8 times
	Base loading	8,580	1 time
	Fatigue cycles of base loading: 278,580; Total fatigue cycles: 367,580		
SL690-402.5	Base loading Marking loading	10,000 5,000	1 time
	Base loading Marking loading	15,000 5,000	1 time
	Base loading Marking loading	10,000 5,000	1 time
	Base loading	3,850	1 time
	Fatigue cycles of base loading: 38,850; Total fatigue cycles: 53,850		

References

[1] J. Schijve, Fatigue of Structures and Materials, Springer, New York, NY, 2008.

[2] X.L. Zhao, FRP-Strengthened Metallic Structures, CRC Press, Boca Raton, Florida, 2013.

[3] A. Mohabeddine, J.A.F.O. Correia, P.A. Montenegro, J.M. Castro, Fatigue crack growth modelling for cracked small-scale structural details repaired with CFRP, Thin-Walled Struct. 161 (2021) 107525, http://dx.doi.org/10.1016/j.tws.2021.107525.

[4] J. Dong, Z. Li, H. Pasternak, Y. Ciupack, Reinforcement of fatigue damaged steel structures using CFRP lamellas - part 3: numerical simulation, Bauingenieur 95 (2021) 362–368, http://dx.doi.org/10.37544/0005-6650-2020-10-32.

[5] P. Feng, L. Hu, X.L. Zhao, L. Cheng, S. Xu, Study on thermal effects on fatigue behavior of cracked steel plates strengthened by CFRP sheets, Thin-Walled Struct. 82 (2014) 311–320, http://dx.doi.org/10.1016/j.tws.2014.04.015.

[6] L.L. Hu, X.L. Zhao, P. Feng, Fatigue behavior of cracked high-strength steel plates strengthened by CFRP sheets, J. Compos. Constr. 20 (2016) 04016043, http://dx.doi.org/10.1061/(asce)cc.1943-5614.0000698.

[7] L. Hu, P. Feng, X.L. Zhao, Fatigue design of CFRP strengthened steel members, Thin-Walled Struct. 119 (2017) 482–498, http://dx.doi.org/10.1016/j.tws.2017.06.029.

[8] H.T. Wang, G. Wu, J.B. Jiang, Fatigue behavior of cracked steel plates strengthened with different CFRP systems and configurations, J. Compos. Constr. 20 (2016) 04015078, http://dx.doi.org/10.1061/(asce)cc.1943-5614.0000647.

[9] L. Li, T. Chen, X. Gu, E. Ghafoori, Heat activated SMA-CFRP composites for fatigue strengthening of cracked steel plates, J. Compos. Constr. 24 (2020) 04020060, http://dx.doi.org/10.1061/(asce)cc.1943-5614.0001072.

[10] M. Mohajer, M. Bocciarelli, P. Colombi, A. Hosseini, A. Nussbaumer, E. Ghafoori, Irreversible cyclic cohesive zone model for prediction of mode I fatigue crack growth in CFRP-strengthened steel plates, Theor. Appl. Fract. Mech. 110 (2020) 102804, http://dx.doi.org/10.1016/j.tafmec.2020.102804.

[11] M. Tavakkolizadeh, H. Saadatmanesh, Fatigue strength of steel girders strengthened with carbon fiber reinforced polymer patch, J. Struct. Eng. 129 (2003) 186–196, http://dx.doi.org/10.1061/(asce)0733-9445(2003)129:2(186).

[12] P. Colombi, Reinforcement delamination of metallic beams strengthened by FRP strips: fracture mechanics based approach, Eng. Fract. Mech. 73 (2006) 1980–1995, http://dx.doi.org/10.1016/j.engfracmech.2006.03.011.

[13] G. Wu, H.T. Wang, Z.S. Wu, H.Y. Liu, Y. Ren, Experimental study on the fatigue behavior of steel beams strengthened with different fiber-reinforced composite plates, J. Compos. Constr. 16 (2012) 127–137, http://dx.doi.org/10.1061/(asce)cc.1943-5614.0000243.

[14] H.T. Wang, G. Wu, Crack propagation prediction of double-edged cracked steel beams strengthened with FRP plates, Thin-Walled Struct. 127 (2018) 459–468, http://dx.doi.org/10.1016/j.tws.2018.02.018.

[15] A. Hosseini, E. Ghafoori, R. Al-Mahaidi, X.L. Zhao, M. Motavalli, Strengthening of a 19th-century roadway metallic bridge using nonprestressed bonded and prestressed unbonded CFRP plates, Constr. Build. Mater. 209 (2019) 240–259, http://dx.doi.org/10.1016/j.conbuildmat.2019.03.095.

[16] E. Ghafoori, M. Motavalli, A. Nussbaumer, A. Herwig, G.S. Prinz, M. Fontana, Design criterion for fatigue strengthening of riveted beams in a 120-year-old railway metallic bridge using pre-stressed CFRP plates, Composites B 68 (2015) 1–13, http://dx.doi.org/10.1016/j.compositesb.2014.08.026.

[17] Z.G. Xiao, X.L. Zhao, CFRP repaired welded thin-walled cross-beam connections subject to in-plane fatigue loading, Int. J. Struct. Stab. Dyn. 12 (2012) 195–211, http://dx.doi.org/10.1142/s0219455412004653.

[18] T. Guo, J. Liu, Y. Deng, Z. Zhang, Fatigue performance of orthotropic steel decks with FRP angles: field measurement and numerical analysis, J. Perform. Constr. Facil. 33 (2019) 04019042, http://dx.doi.org/10.1061/(asce)cf.1943-5509.0001308.

[19] J. Liu, T. Guo, D. Feng, Z. Liu, Fatigue performance of rib-to-deck joints strengthened with FRP angles, J. Bridge Eng. 23 (2018) 04018060, http://dx.doi.org/10.1061/(asce)be.1943-5592.0001286.

[20] C. Wu, X.L. Zhao, R. Al-Mahaidi, M.R. Emdad, W. Duan, Fatigue tests of cracked steel plates strengthened with UHM CFRP plates, Adv. Struct. Eng. 15 (2012) 1801–1815, http://dx.doi.org/10.1260/1369-4332.15.10.1801.

[21] A. Hosseini, E. Ghafoori, M. Motavalli, A. Nussbaumer, X.L. Zhao, Mode I fatigue crack arrest in tensile steel members using prestressed CFRP plates, Compos. Struct. 178 (2017) 119–134, http://dx.doi.org/10.1016/j.compstruct.2017.06.056.

[22] R. Emdad, R. Al-Mahaidi, Effect of prestressed CFRP patches on crack growth of centre-notched steel plates, Compos. Struct. 123 (2015) 109–122, http://dx.doi.org/10.1016/j.compstruct.2014.12.007.

[23] A. Hosseini, A. Nussbaumer, M. Motavalli, X.L. Zhao, E. Ghafoori, Mixed mode I/II fatigue crack arrest in steel members using prestressed CFRP reinforcement, Int. J. Fatigue 127 (2019) 345–361, http://dx.doi.org/10.1016/j.ijfatigue.2019.06.020.

[24] E. Lepretre, S. Chataigner, L. Dieng, L. Gaillet, Fatigue strengthening of cracked steel plates with CFRP laminates in the case of old steel material, Constr. Build. Mater. 174 (2018) 421–432, http://dx.doi.org/10.1016/j.conbuildmat.2018.04.063.

[25] P. Colombi, A. Bassetti, A. Nussbaumer, Delamination effects on cracked steel members reinforced by prestressed composite patch, Theor. Appl. Fract. Mech. 39 (2003) 61–71, http://dx.doi.org/10.1016/s0167-8442(02)00138-6.

[26] S. Mall, D.S. Conley, Modeling and validation of composite patch repair to cracked thick and thin metallic panels, Composites A 40 (2009) 1331–1339, http://dx.doi.org/10.1016/j.compositesa.2008.08.007.

[27] Y. Zheng, Experimental and Theoretical Research on Fatigue Behavior of Steel Structures Strengthened with CFRP (Doctoral Dissertation), Tsinghua University, Beijing, 2007.

[28] C.S. Hansen, P.H. Jensen, J. Dyrelund, B. Täljsten, Crack propagation on ESE(T) specimens strengthened with CFRP sheets, in: Advanced Composites in Conctruction (2009): Conference Proceedings, NetComposites Limited, Chesterfield, Great Britan, 2009, pp. 402–413.

[29] B. Zheng, M. Dawood, Debonding of carbon fiber–reinforced polymer patches from cracked steel elements under fatigue loading, J. Compos. Constr. 20 (2016) 04016038, http://dx.doi.org/10.1061/(asce)cc.1943-5614.0000694.

[30] A.A. Baker, Repair efficiency in fatigue-cracked aluminium components reinforced with boron/epoxy patches, Fatigue Fract. Eng. Mater. Struct. 16 (1993) 753–765, http://dx.doi.org/10.1111/j.1460-2695.1993.tb00117.x.

[31] Y. Huawen, C. König, T. Ummenhofer, Q. Shizhong, R. Plum, Fatigue performance of tension steel plates strengthened with prestressed CFRP laminates, J. Compos. Constr. 14 (2010) 609–615, http://dx.doi.org/10.1061/(asce)cc.1943-5614.0000111.

[32] H.T. Wang, G. Wu, Bond–slip models for CFRP plates externally bonded to steel substrates, Compos. Struct. 184 (2018) 1204–1214, http://dx.doi.org/10.1016/j.compstruct.2017.10.033.

[33] D. Fernando, J.G. Teng, T. Yu, X.L. Zhao, Preparation and characterization of steel surfaces for adhesive bonding, J. Compos. Constr. 17 (2013) 04013012, http://dx.doi.org/10.1061/(asce)cc.1943-5614.0000387.

[34] X.L. Zhao, Y. Bai, R. Al-Mahaidi, S. Rizkalla, Effect of dynamic loading and environmental conditions on the bond between CFRP and steel: state-of-the-art review, J. Compos. Constr. 18 (2014) A4013005, http://dx.doi.org/10.1061/(asce)cc.1943-5614.0000419.

[35] Q.Q. Yu, R.X. Gao, X.L. Gu, X.L. Zhao, T. Chen, Bond behavior of CFRP-steel double-lap joints exposed to marine atmosphere and fatigue loading, Eng. Struct. 175 (2018) 76–85, http://dx.doi.org/10.1016/j.engstruct.2018.08.012.

[36] Y. Pang, G. Wu, H. Wang, Z. Su, X. He, Experimental study on the bond behavior of CFRP-steel interfaces under quasi-static cyclic loading, Thin-Walled Struct. 140 (2019) 426–437, http://dx.doi.org/10.1016/j.tws.2019.03.060.

[37] Y. Doroudi, D. Fernando, V.T. Nguyen, J.P. Torres, Experimental study on CFRP-to-steel bonded interfaces under quasi-static cyclic loading, J. Compos. Constr. 23 (2019) 04019023, http://dx.doi.org/10.1061/(asce)cc.1943-5614.0000945.

[38] H.T. Wang, G. Wu, Y.Y. Pang, J.W. Shi, H.M. Zakari, Experimental study on the bond behavior between CFRP plates and steel substrates under fatigue loading, Composites B 176 (2019) 107266, http://dx.doi.org/10.1016/j.compositesb.2019.107266.

[39] P. Colombi, G. Fava, Fatigue behaviour of tensile steel/CFRP joints, Compos. Struct. 94 (2012) 2407–2417, http://dx.doi.org/10.1016/j.compstruct.2012.03.001.

[40] O. Buyukozturk, O. Gunes, E. Karaca, Progress on understanding debonding problems in reinforced concrete and steel members strengthened using FRP composites, Constr. Build. Mater. 18 (2004) 9–19, http://dx.doi.org/10.1016/s0950-0618(03)00094-1.

[41] J.J. Denney, S. Mall, Characterization of disbond effects on fatigue crack growth behavior in aluminum plate with bonded composite patch, Eng. Fract. Mech. 57 (1997) 507–525, http://dx.doi.org/10.1016/s0013-7944(97)00050-7.

[42] M. Bocciarelli, P. Colombi, T. D'Antino, G. Fava, Intermediate crack induced debonding in steel beams reinforced with CFRP plates under fatigue loading, Eng. Struct. 171 (2018) 883–893, http://dx.doi.org/10.1016/j.engstruct.2018.04.002.

[43] Q.Q. Yu, X.L. Zhao, T. Chen, X.L. Gu, Z.G. Xiao, Crack propagation prediction of CFRP retrofitted steel plates with different degrees of damage using BEM, Thin-Walled Struct. 82 (2014) 145–158, http://dx.doi.org/10.1016/j.tws.2014.04.006.

[44] H. Liu, X.L. Zhao, R. Al-Mahaidi, Boundary element analysis of CFRP reinforced steel plates, Compos. Struct. 91 (2009) 74–83, http://dx.doi.org/10.1016/j.compstruct.2009.04.032.

[45] H. Liu, R. Al-Mahaidi, X.L. Zhao, Experimental study of fatigue crack growth behaviour in adhesively reinforced steel structures, Compos. Struct. 90 (2009) 12–20, http://dx.doi.org/10.1016/j.compstruct.2009.02.016.

[46] Y. Zheng, L. Hu, Y. Wang, P. Feng, Fatigue life of CFRP laminate strengthened high-strength steel plates under fatigue loadings, IOP Conf. Ser.: Mater. Sci. Eng. 768 (2020) 032040, http://dx.doi.org/10.1088/1757-899x/768/3/032040.

[47] H. Liu, Z. Xiao, X.L. Zhao, R. Al-Mahaidi, Prediction of fatigue life for CFRP-strengthened steel plates, Thin-Walled Struct. 47 (2009) 1069–1077, http://dx.doi.org/10.1016/j.tws.2008.10.011.

[48] P. Colombi, G. Fava, L. Sonzogni, Fatigue crack growth in CFRP-strengthened steel plates, Composites B 72 (2015) 87–96, http://dx.doi.org/10.1016/j.compositesb.2014.11.036.

[49] Y. Zheng, Y. Wang, L. Hu, P. Feng, Crack propagation and debonding development of CFRP laminate strengthened high-strength steel plates under fatigue loadings, IOP Conf. Ser.: Mater. Sci. Eng. 768 (2020) 032047, http://dx.doi.org/10.1088/1757-899x/768/3/032047.

[50] Matlab, Neural Networks Toolbox Release R2019a, The MathWorks, Inc., Natick, Massachusetts, United States, 2019.

[51] C.A. Brebbia, J. Dominguez, Boundary Element: An Introductory Course, WIT Press, Boston, MA, 1992.

[52] W.S. Hall, The Boundary Element Method, Kluwer Academic Publishers, Cleveland, UK, 1994.

[53] F.R. Mashiri, X.L. Zhao, P. Grundy, Crack propagation analysis of welded thin-walled joints using boundary element method, Comput. Mech. 26 (2000) 157–165, http://dx.doi.org/10.1007/s004660000163.

[54] Computational Mechanics BEASY Ltd, Beasy User's Guide for Revision 9.0, Computational Mechanics BEASY Ltd, Ashurst, Southampton, 2006.

[55] Y. Wang, Fatigue Debonding Experiment and Boundary Element Simulation of Steel Plates Strengthened with CFRP (Master Thesis), China University of Mining and Technology, Beijing, China.

[56] Y. Pang, Study on the Bond Behavior of CFRP-Steel Interfaces under Extreme Service Environment (Doctor Thesis), Southeast University, Nanjing, China.

[57] Fatigue Crack Growth Computer Program NASGRO Version 3.0-Reference Manual, Rapp. Tecn. JSC-22267, NASA, 2001.

[58] J.C. Newman, A crack opening stress equation for fatigue crack growth, Int. J. Fract. 24 (1984) R131–R135, http://dx.doi.org/10.1007/bf00020751.

[59] British Standards Institution, Guide to Methods for Assessing the Acceptability of Flaws in Metallic Structures, BSI, London, 2005.

[60] International Institute of Welding, Recommendations for Fatigue Design of Welded Joints and Components, IIW Document IIW-1823-07 ex XIII-2151-07/XV-1254-07, IIW Annual Assembly, Graz, Austria, 2008.